RSC Advances

PAPER

Cite this: *RSC Adv.*, 2022, **12**, 11885

Stepwise copolymerization of polybenzimidazole for a low dielectric constant and ultrahigh heat resistance†

Xianzhu Zhong, [a] Aniruddha Nag, [ac] Jiabei Zhou,[a] Kenji Takada, [a] Fitri Adila Amat Yusof,[b] Tetsu Mitsumata,[b] Kenji Oqmhula,[a] Kenta Hongo, [a] Ryo Maezono[a] and Tatsuo Kaneko *[a]

Received 7th March 2022
Accepted 9th April 2022

DOI: 10.1039/d2ra01488b

rsc.li/rsc-advances

Bio-based polymer materials having great potential due to the depletion of fossil-fuel resources have been applied as single-use and medicinal materials but their low thermomechanical resistance have limited wider applications. Here, ultrahigh thermoresistant bio-based terpolymers with a low dielectric constant, comprising polybenzimidazole and poly(benzoxazole-*random*-aramid), were prepared by a method involving stepwise polycondensation of three monomers, 3,4-diaminobenzoic acid for benzimidazoles, 3-amino-4-hydroxylbenzoic acid for benzoxazoles, and 4-aminobenzoic acid for aramids. For optimized monomer compositions, the obtained terpolymers exhibited dielectric constants lower than 3, and a 10% mass loss at approximately 760 °C which is a temperature higher than that for any other polymer material reported so far. The high thermal degradation temperatures of the prepared terpolymers were a result of the high interaction enthalpies of hydrogen bonding between imidazole rings in the polymer chains, which were obtained from density functional theory calculations using trimer models. Furthermore, the applicability of the prepared terpolymers as a wire-coating material for a simple motor insulation was demonstrated, indicating that it has significant potential to be used as a thermostable material with a low dielectric constant (k).

1. Introduction

Bio-based polymer materials developed from natural resources are sustainable and reliable, and therefore an ideal alternative to petroleum-based polymer materials.[1–5] Bio-based materials, such as poly(lactic acid) (PLA) and polyhydroxybutyrates (PHB), have been developed and used for various applications.[3,6,7] However, as most bio-based polymer materials have a low thermal resistance and poor electric function, they cannot be applied as engineering plastics that need to function in extreme conditions, such as in aerospace and electric vehicles, and high-power engines.[8–10]

Bio-based polybenzimidazole (PBI), which exhibits excellent thermal resistance, has been previously synthesized from 3,4-diaminobenzoic acid (DABA) *via* the Smiles rearrangement of the hydroxyl group of fermented 3-amino-4-hydroxybenzoic acid (AHBA).[11,12] In addition, poly(benzimidazole-*co*-amide) (PBI-*co*-PA) was synthesized by introducing amide groups to increase the processability of the polymer. Interestingly, it was found that the thermal decomposition temperature of PBI-*co*-PA increased with the incorporation of a small amount of PA (up to 15 mol%), in spite of the low degradation temperature of the PA units. Another PBI copolymer, poly(benzimidazole-*co*-benzoxazole) (PBI-*co*-PBO) was synthesized through the copolymerization of DABA with AHBA. This copolymer exhibited excellent low dielectric constant (low-k) performance; however, its thermal stability and processability were not optimized.[13] Therefore, the development of a PBI derivative as a processable polymer material with outstanding thermal resistance and low-k performance remains a significant challenge.[9,14–17]

In this work, we design a series of PBI derivatives possessing improved thermal, mechanical and dielectric properties, by incorporating aramid and benzoxazole components into PBI. Among these derivatives, a terpolymer of appropriate composition exhibits a significant low k, as well as an ultrahigh thermodegradation temperature that is much higher than those of conventional polymers, including PBI and PBO.

2. Experimental section

2.1. Materials

AHBA (purity: >97%), DABA (purity: 98%), 4-aminobenzoic acid (PABA) (purity: >99%), and sodium hydroxide (NaOH) (purity:

[a]Graduate School of Advanced Science and Technology, Energy and Environment Area, Japan Advanced Institute of Science and Technology (JAIST), 1-1 Asahidai, Nomi, Ishikawa, 923-1292, Japan. E-mail: kaneko@jaist.ac.jp

[b]Department of Materials Science & Technology, Faculty of Engineering, Niigata University, Ikarashi, Nishi-ku, Niigata, 950-2181, Japan

[c]School of Energy Science and Engineering, Vidyasirimedhi Institute of Science and Technology, Rayong 21210, Thailand

† Electronic supplementary information (ESI) available. See https://doi.org/10.1039/d2ra01488b

>98%) were purchased from TCI (Tokyo Chemical Industry). Poly(phosphoric acid) (PPA) (purity: 85%) was obtained from Sigma-Aldrich. Methane sulfonic acid (MSA) (purity: >98%) and trifluoroacetic acid (TFA) (purity: >98%) were supplied by Wako pure chemical Industries, Ltd. pH test paper, supplied by (Macherey-Nagel GmbH & Co. KG, Düren, Germany). Copper wire were purchased from SENKO Co., Ltd. All the solvents and reagents in this research were used as received without any further processing or purification.

2.2. Syntheses

2.2.1. Monomers. DABA used in this work was synthesized from AHBA, which was obtained from nonedible cellulosic biomass. In the synthetic pathway, Smiles rearrangement was adopted to change the hydroxyl group into amine group, the specific synthesis information was reported in previous research.[13] DABA (6.0 g, 31.5 mmol) was dispersed in 30 mL methanol and kept stirring. Hydrochloric acid (12 N) was added dropwise to the suspension until DABA was completely dissolved, after the color changed from pink to dark red, kept stirring at room temperature for 4 h. The pink salt of DABA dihydrochloride (DABA·2HCl) was obtained *via* solvent rotary-evaporation (yield: 5.4 g, 94%). AHBA hydrochloride (AHBA·HCl) and PABA acid hydrochloride (PABA·HCl) salts were obtained following the same method as of DABA.

2.2.2. Synthesis of PBI–PBO–PA *via* one-pot terpolymerization. To synthesize the terpolymer, a simple polymerization reaction was performed, in which DABA·2HCl, AHBA·HCl, and PABA·HCl were simultaneously added to the reaction system. The terpolymers were synthesized in PBI–PBO–PA compositions (mol%) of 70–30–0, 70–27–3, 70–21–9, 70–15–15, 70–9–21, 70–3–27 and 70–0–30, respectively. The synthesis of the terpolymer with a composition of 70–21–9 (mol%) is described below as a representative synthetic procedure. Herein, 25 g of PPA was taken in a three-necked round-bottomed flask with a magnetic stirrer and heated at 100 °C for 1 h in a nitrogen atmosphere to remove any traces of moisture. Subsequently, DABA·HCl (940.8 mg, 4.20 mmol), AHBA·HCl (239.4 mg, 1.26 mmol), and PABA·HCl (93.9 mg, 0.54 mmol) were added to the flask, and the contents were stirred continuously for 1 h until all the moisture was eliminated, and the monomeric solids were completely dissolved in the reaction system. The mixture was then successively heated at 160 °C, 180 °C, and 200 °C for 4 h each, and ultimately at 220 °C for 12 h, during which the color of the solution changed from red to dark brown. The resultant solution was dispersed in water and stirred for 12 h to remove PPA; subsequently, a brown solid was obtained on filtration. After drying under vacuum, the solid was ground into a powder and suspended in deionized water. Then, 1 M NaOH was slowly added, and the solution was stirred until the pH of the solution reached 7.0, and it was maintained for 1 h. The solid was collected by filtration and dried under vacuum to obtain a brown powder (601.0 mg, 5.16 mmol) as the final product. An analogous synthetic process was performed for each of the terpolymers with other molar ratios. The yields for the syntheses of terpolymers with in-fed compositions (mol%) of 70–30–0, 70–27–3, 70–21–9, 70–15–15, 70–9–21, 70–3–27 and 70–0–30 are 91%, 89%, 86%, 87%, 82%, 86% and 89%, respectively.

2.2.3. Synthesis of PBI–PBO–PA *via* stepwise terpolymerization. Terpolymers were also synthesized using another method. The terpolymers were synthesized having the same BI-BO-A molar compositions with the one-pot terpolymerization. The terpolymer in composition of 70–21–9 (mol%) is described below as a representative synthetic procedure. Pre-polymerization of DABA was performed to prepare the polybenzimidazole homopolymer at the first synthetic step of the terpolymer, poly(benzimidazole-*block*-benzoxazole-*random*-aramid) (P(BI-*b*-BO-A)). Further, 25 g of PPA was taken in a three-necked round-bottomed flask with a magnetic stirrer, and heated at 100 °C for 1 h in a nitrogen gas atmosphere to remove any traces of moisture. Then, DABA·HCl (940.8 mg, 4.2 mmol) was slowly added to PPA, and the suspension was stirred for 1 h. The temperature was then raised to 180 °C, and stirring was continued for another 1 h to increase the viscosity, which indicated the polymerization of DABA to some extent.[16] Subsequently, the reaction system was cooled to 100 °C, and AHBA·HCl (239.4 mg, 1.26 mmol), and PABA·HCl (93.9 mg, 0.54 mmol) were added to the flask. The contents were stirred continuously for 1 h until all the moisture was removed and the monomeric solids were completely dissolved in the reaction system. The mixture was then heated successively at 160 °C, 180 °C, and 200 °C for 4 h each and ultimately at 220 °C for 12 h, during which the color of the solution changed from red to dark brown. The resulting liquid was poured into water and stirred for 12 h to remove PPA; subsequently, a brown solid was obtained on filtration. After drying under vacuum, the solid was ground into a powder and suspended in deionized water. Subsequently, 1 M NaOH (10%) was slowly added with stirring until the pH of the solution reached 7.0; it was maintained for 1 h. The solid was collected by filtration and dried under vacuum, and a brown powder (643.0 mg, 5.52 mmol) was obtained as the final product. An analogous synthetic process was performed for each of the terpolymers with other molar ratios. The yields for the syntheses of terpolymers with in-fed compositions (mol%) of 70–30–0, 70–27–3, 70–21–9, 70–15–15, 70–9–21, 70–3–27 and 70–0–30 are 85%, 87%, 92%, 90%, 88%, 83% and 87%, respectively.

2.2.4. Film fabrication. The cast of poly(BI-*b*-BO-A) (100.0 mg, 0.2 mmol) was made over TFA solution (3 mL) containing 2 drops of MSA on a silicon wafer. After drying at 25 °C (to evaporate the TFA), the film was scratched off the substrate and then immersed in deionized water for 12 h to remove the residual acid. The film was obtained after dried in 80 °C.

2.3. Measurements

Fourier transform infrared (FT-IR) spectra of terpolymers were recorded in a PerkinElmer Spectrum with a diamond-attenuated total reflection (ATR) accessory. The wavenumber range was set as 4000 to 400 cm^{-1}. Solid-state ^{13}C NMR CP/TOSS (Total Suppression of Spinning Sidebands) spectra of the terpolymer were recorded with a Bruker Advance III

spectrometer operating at 125 MHz. Terpolymer samples were filled into 7 mm diameter zirconia rotor with a Kel-F cap and then spun at 8 kHz. The contact time and the period between successive accumulations were set as 2 s and 5 s respectively. The total number of the scans was set as 25 000.

The viscosity of terpolymer was measured through a viscometer SIBATA 026300-3. Conc. sulfuric acid (H_2SO_4) was used as a solvent. Thermo-gravimetric analysis (TGA) curves of the terpolymers were recorded using a HITACHI STA7200. In a platinum crucible, the samples (5 mg) were placed and heated under a nitrogen atmosphere to 1000 °C with a heating rate of 10 °C min^{-1}. The 5% mass loss temperature (T_{d5}) and 10% mass loss temperature (T_{d10}) of the samples were taken as indices of the thermal decomposition temperatures.

The stress–stain curves of the terpolymers were recorded *via* tensile mode mechanical tests using an Instron-3365 mechanical tester instrument at room temperature. Samples were shaped into a rectangular film with a length of 40 mm, width of 7 mm and a thickness of 15 μm. The elongation speed was set as 0.4 mm min^{-1}.

The electrical resistivity of the terpolymer films was measured using a digital megohmmeter (DSM-8104 HIOKI) at 25 °C. External electromagnetic noise was shielded by a Faraday cage during the measurement. Through conductive rubber electrodes with a guard electrode, two terminal methods were adopted to apply 1 kV DC electric voltage to the film which had dimensions of 40 × 40 mm. The formula $\rho_v = (S/t) \times R_m$ was used to calculate the volume resistivity ρ_v (Ω cm), where S is the area of the electrode, t represents the thickness of the film.

The crystallinity was investigated using an X-ray diffractometer (SmartLab; Rigaku Corp., Akishima, Japan). Wide-angle X-ray diffraction (WAXD) patterns was checked from the facade of the film with a graphite-monochromatized Cu Kα radiation beam generated at 100 mA and 40 kV.

The measurement of dielectric constant of the terpolymer films were carried out in an LCR meter (HIOKI IM3536) at 20 °C with a frequency of 1 MHz. The measurement was carried out by two terminals method with an applied electric potential of 1.0 V. The film was sandwiched between two electrodes with a constant pressure of 86 kPa and the sample holder was set in a Faraday cage. The relative dielectric constant (k_r) was calculated *via* the formula of $k_r = Cd/k_0A$, where C is the capacitance, d is thickness of film, A is the cross-sectional area of film and k_0 is the dielectric constant in vacuum (=8.854 × 10^{-12} F m^{-1}).

The coating experiment was performed using the copper wire with a diameter of 0.6 mm. The assembled mini motor is powered by 2 batteries of 1.5 V. In the experiment of heat resistance of PBI–PBO–PA coating, two copper wires coated with terpolymer were connected with a sample holder made of strainless-steel in a parallel circuit. An electrical potential of 10.0 V was applied to the circuit using a dc power supply (PWR200MH KIKUSUI). Both copper wires were approximately 8.0 cm long, therefore the electric current flowed could be same for both wires. The electric current flowed in the main circuit was measured to be 16.0 A.

2.4. Theoretical calculations

To understand thermal stability of the terpolymer, we made several trimer models and evaluated their interaction enthalpies of the H-bonds between molecular chains theoretically, following our previous study:[13] All the DFT simulations were carried out using Gaussian 16.[18] To properly describe the charge transfer relevant to the H-bonds, CAM-B3LYP was chosen as the exchange-correlation functional,[19] associating with the cc-pVQZ basis set.[20] A basis-set superposition error was reduced by applying the counterpoise correction to optimize each of the geometries.[21]

3. Results and dicussions

3.1. Syntheses

Terpolymers were synthesized in bulk by a one-pot polymerization method. Although the polymerization mixture became viscous and the reaction appeared successful, casting of the resulting polymers did not produce self-standing films, as can be seen from the photograph in the inset of Scheme 1. If the macromolecular backbone is too rigid, processing becomes difficult in some cases. Considering the good processability of

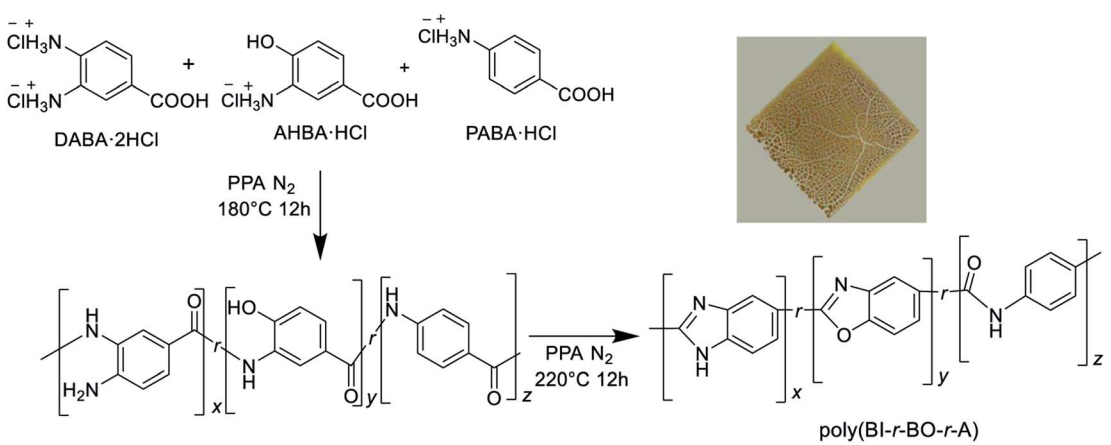

Scheme 1 Synthetic pathway of terpolymers from three aminobenzoic acid derivatives through simple polymerization. Inset: picture of cast film.

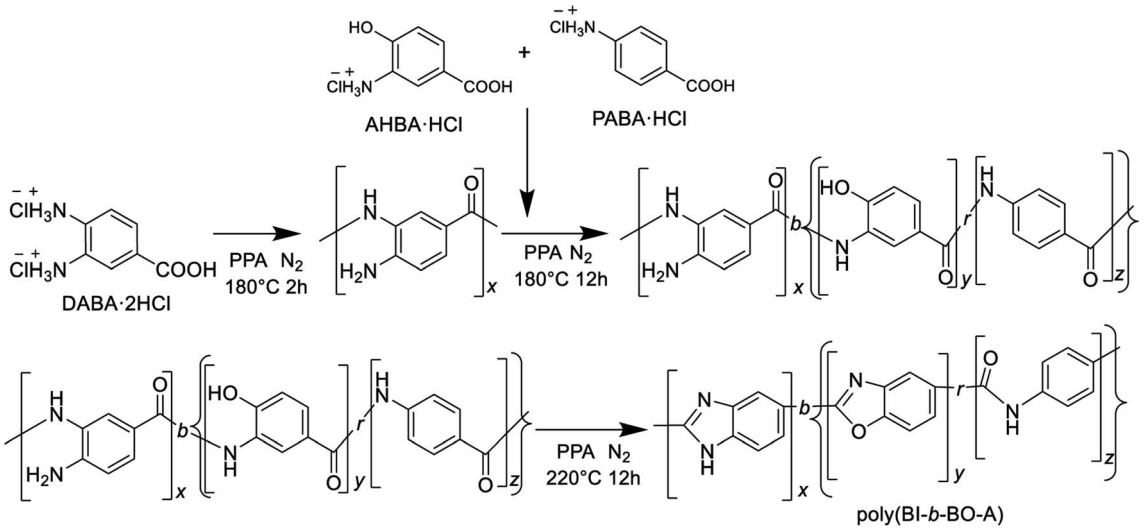

Scheme 2 Synthetic pathway of P(BI-*b*-BO-A) from three aminobenzoic acid derivatives through stepwise polymerization.

PBI, as shown in previous reports,[9,13] it was hypothesized that the continuous structure of benzimidazole units might be effective for film preparation.

Therefore, a stepwise method was adopted for the synthesis; at first, the polybenzimidazoles were synthesized for short-range polymerization; then, the monomers for PBO and PA were added and successively polymerized to produce poly(BI-*b*-BO-A), as shown in Scheme 2.

The self-standing film was successfully fabricated, and the film was further dried at 80 °C for 12 h (Fig. 1a). The film was pliable enough to be folded into the shape of an origami airplane (Fig. 1b); after unfolding, it did not tear or break (Fig. 1c).

The structures of the polymers were confirmed by Fourier Transform-Infrared (FT-IR) and ^{13}C solid-state Nuclear Magnetic Resonance (NMR) spectroscopies. In the FT-IR spectra (Fig. S1†), for terpolymer in all the ratios, distinct C=N, C=C, and C–N absorption peaks were observed at approximately 1690 cm^{-1}, 1590 cm^{-1} and 1380 cm^{-1} respectively. Besides, the C=O absorption peaks gradually showed at approximately 1745 cm^{-1} and became stronger as PA ratio increasing from 0 to 30%, but the C–O peaks became weaker and vanished ultimately because of the decreasing composition of PBO. In the solid-state NMR spectrum (Fig. 2), six distinct signals in the range of 100 to 180 ppm and some very broad signals between 190 and 220 ppm were detected. The signal at 167 ppm was assigned to oxazole carbon (marked as 5), and the signal at 160 ppm contained the imidazole carbon (marked as 1) among others. Very broad signals in the range of 190 to 220 ppm were assigned to amide carbonyl carbons that connect BI and BO to A. The other signals were assigned to the benzene carbons. The close resemblance between the solid-state NMR spectra of the polymers synthesized *via* one-pot and stepwise polymerization, suggested that they had analogous structures.

The NMR signal from the carbon marked as 4 (C_4), is expected to be sensitive to the presence of neighboring units such as BI, BO, and A. Therefore, the broadness of this signal for the polymer prepared by simple polymerization can be attributed to the presence of all the three neighboring units around C_4. In contrast, the sharper C_4 signal detected for the polymer prepared by stepwise polymerization can be explained by the PBI block formation.

The molecular weight of the polymers could not be evaluated by chromatography owing to their poor solubility in popular

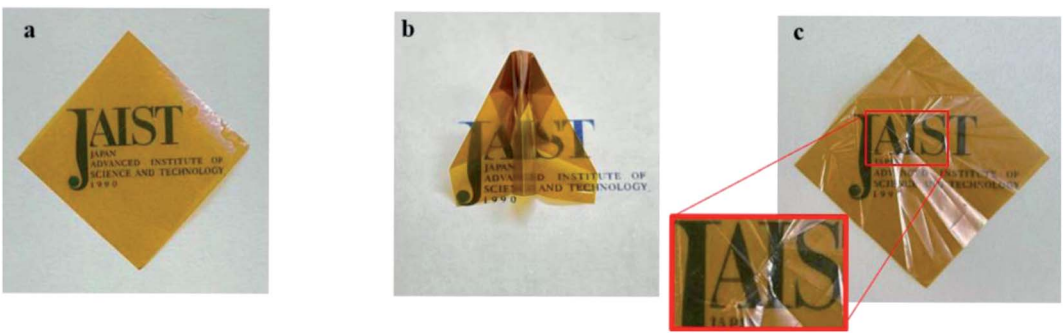

Fig. 1 Images of the solution casted film of terpolymer. (a) Pristine, (b) origami-folded, and (c) unfolded films.

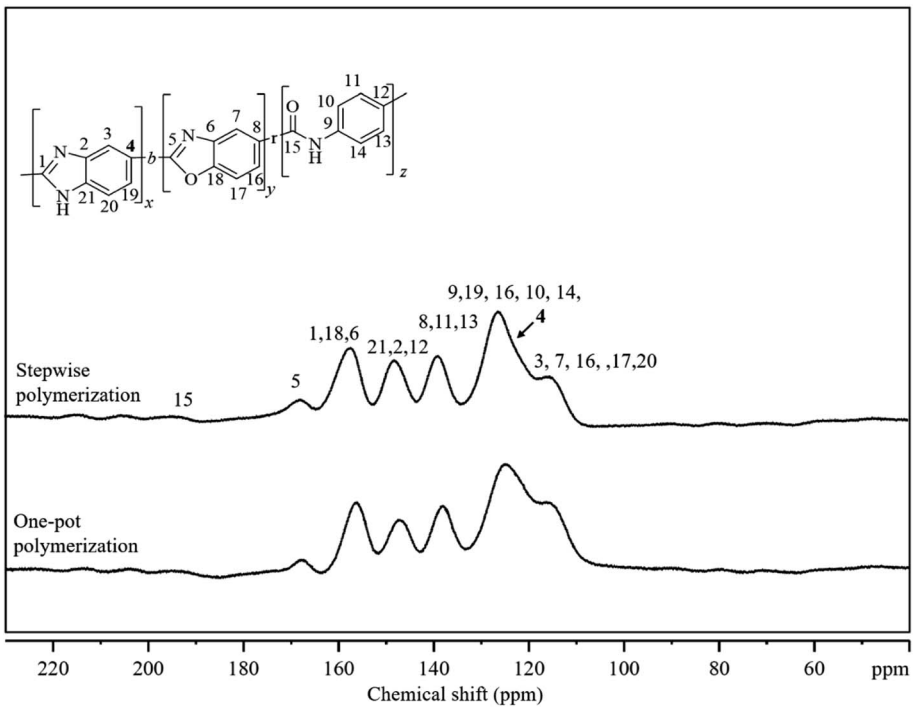

Fig. 2 Solid-state ^{13}C CP/TOSS NMR spectra of terpolymers in 70–21–9 (mol%) prepared by a one-pot polymerization and a stepwise polymerization method.

solvents. However, the inherent viscosities (η_{inh}) of the polymers were evaluated in a solution of concentrated sulfuric acid to compare their degrees of polymerization, as described in Table 1.

The inherent viscosities of terpolymers synthesized by stepwise polymerization (η_{inh1}) ranged from 1.24 to 1.89 dL g^{-1}, which are much higher than those of the terpolymers synthesized by simple polymerization (η_{inh2}: 0.64–0.84 dL g^{-1}). DABA possesses a high polymerizability owing to the reactive functional groups of *o*-diamine. The higher values of η_{inh1} compared to η_{inh2} are responsible for the formation of the pliable film from P(BI-*b*-BO-A) (Fig. 1). In addition, η_{inh} decreases with a decrease in the amount of PBO (and increase in PA) for both types of terpolymers. This can be attributed to the higher amine reactivity due to the presence of the *o*-hydroxy groups.

3.2. Thermal properties

The thermal stabilities of the terpolymers synthesized by stepwise polymerization were estimated using thermogravimetric analysis (TGA) under a nitrogen atmosphere. According to the thermograms obtained (Fig. 3a), none of the terpolymers were found to exhibit any significant loss of mass up to ~520 °C; mass loss started occurring at approximately 550 °C. Significant mass losses were observed with an increase in temperatures up to 1000 °C. Interestingly, the completion of thermal degradation was not detected below 1000 °C, and the residue yields were still higher than 69 wt%. The thermal decomposition temperatures T_{d5} and T_{d10} for P(BI-*b*-BO-A) of all compositions have been listed in Table 1 and plotted against the PA compositions in Fig. 3b. Both T_{d5} and T_{d10} were almost constant for low mole

Table 1 Thermal and mechanical properties of bio-based terpolymers

Polymer[a] composition (%)	T_{d5}[b] (°C)	T_{d10}[b] (°C)	σ[c] (MPa)	γ[c] (%)	E[c] (GPa)	η_{inh1} (η_{inh2})[d] (dL g^{-1})
70–30–0	638	703	80 ± 1.5	2.3 ± 0.1	3.48	1.89 (0.84)
70–27–3	634	701	76 ± 3.2	3.2 ± 0.2	2.38	1.75 (0.78)
70–21–9	624	707	76 ± 1.0	5.1 ± 0.1	1.49	1.65 (0.77)
70–15–15	637	716	74 ± 1.4	6.7 ± 0.1	1.23	1.38 (0.78)
70–9–21	658	736	72 ± 1.2	8.6 ± 0.1	0.84	1.30 (0.75)
70–3–27	675	758	63 ± 1.7	10.3 ± 0.1	0.61	1.28 (0.74)
70–0–30	686	763	48 ± 1.6	12.0 ± 0.2	0.40	1.24 (0.64)

[a] Terpolymers in varying compositions of PBO and PA, in which PBO varied from 30% to 0 while PA composition varied from 0 to 30%. PBI composition were fixed at 70%. [b] Thermal property indices, measured by TGA at nitrogen atmosphere. 5% and 10% weight loss thermal decomposition temperatures (T_{d5} and T_{d10}). [c] Mechanical properties σ, γ, and E measured by stress–strain tensile test refer to tensile strength at break, strain at beak, and Young's modulus, respectively. [d] η_{inh1} refers to inherent viscosity of terpolymer synthesized by stepwise polymerization, while η_{inh2} shown in parentheses refers to inherent viscosity of terpolymer synthesized *via* one-pot polymerization.

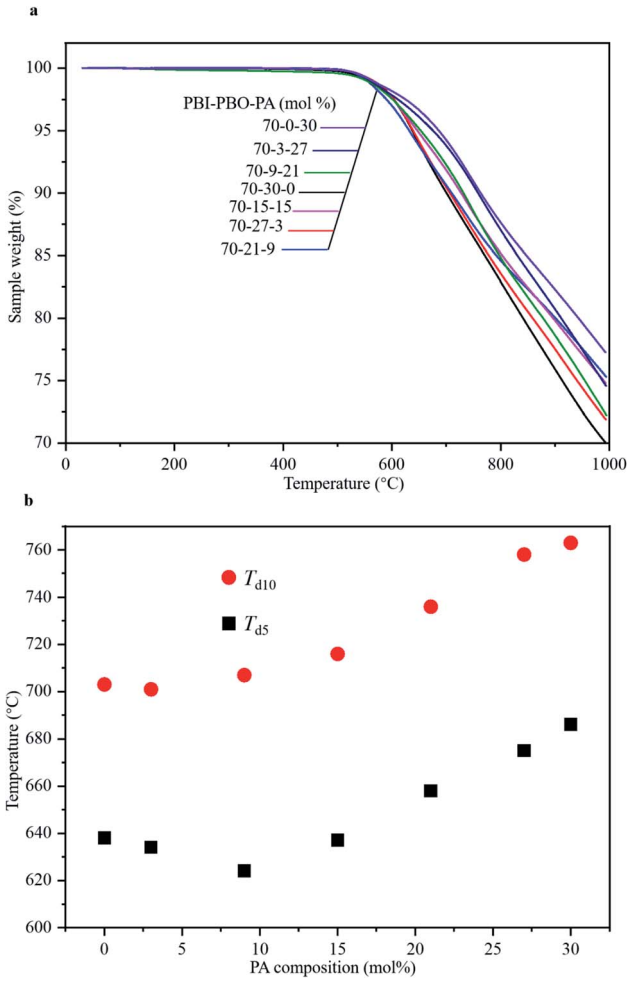

Fig. 3 Thermal characterization of terpolymers. (a) TGA curves of terpolymers with various compositions. (b) T_{d5} and T_{d10} of terpolymers of different compositions.

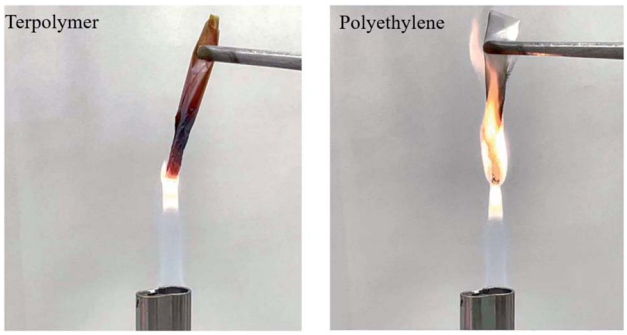

Fig. 4 Burning photographs depicting the burning terpolymer (left) and polyethylene (right).

percentages of PA. However, beyond a critical PA composition of 9 mol%, they gradually increased with increasing mol% of PA. Terpolymers having 30 mol% of PA showed the highest T_{d5} and T_{d10} values of 686 °C and 763 °C, respectively. This can be attributed to the occurrence of inter-chain hydrogen bonds between the imidazoles and primary amines, which increase in number with the increase in relative mol% of PA compared to benzoxazoles. Overall, the terpolymers were found to exhibit ultrahigh thermal stability, and a T_{d10} of ~760 °C, which is the highest value reported so far for plastic films, and is comparable to the melting points of light metals such as aluminum and magnesium.

The burning characteristics of the terpolymers were investigated using a combustion test, in which a terpolymer film with a composition of 70%–21%–9% was taken as the representative terpolymer and a polyethylene film was used as the reference. A visual of the entire burning process can be found in Video S1.† Unlike that for the polyethylene film, no obvious flame was visible during the burning of the terpolymer film (Fig. 4). In addition, the ignition of the terpolymer film was quenched immediately after removal from the fire, and no dripping of the material was observed during the entire test, suggesting that the terpolymer film is extremely flame-retardant.

To elucidate the mechanism of thermal stability of the terpolymer, the interaction enthalpy of the hydrogen bonds (H-bonds) between its molecular chains was investigated *via* density functional theory (DFT) calculations. Several trimer models comprising three units of 2-phenylbenzimidazole (2BI), 2-phenylbenzoxazole (2BO), and benzanilide (BA) were used to simulate the polymer chains. Since PBI had the highest composition (70 mol%) in our terpolymers, the interaction enthalpy of the hydrogen bonding between imidazole N–H (model 1) and imidazole N (model 2) were calculated in detail. The results have been presented in Table 2. The interaction enthalpy for H-bonding between the two BI primary models was calculated to be −13.32 kcal mol^{-1}, which was higher than that calculated for any other combination of BI, BO and BA primary models (entries 1–5). The results indicate that the H-bonding between two imidazole rings is the strongest of the five combinations. Next, the models were extended to trimers with BI as the central unit. In a previous work from our group, the H-bonding between two models of BI-BI-BI was found to be very weak (with an interaction enthalpy of −4.77 kcal mol^{-1}), presumably due to the lowered reactivity of both N–H and –N= by resonance stabilization in the long π-conjugation (entry 6).[13] However, the incorporation of BA in either one of the two trimer models was found to increase the H-bond interaction enthalpies (entries 7-10). In the present study, it was observed that the H-bonding was strengthened by the incorporation of BO and BA on both sides of the central BI. The interaction enthalpy between the two trimer models of BA-BI-BA (entry 11) was estimated to be −14.13 kcal mol^{-1}, which is slightly higher than that of entry 1, owing to the limitation of resonance stabilization, and the possible induction effects due to the substitution with BA. For BO-BI-BO and BO-BI-BA, the H-bonding enthalpies were calculated to be −13.57 kcal mol^{-1} and −13.80 kcal mol^{-1}, respectively. The absolute values of the H-bonding interaction enthalpies were found to increase with increase in the amount of incorporated PA, indicating an elevation in the interaction enthalpy of the H-bond due to the incorporation of PA into PBI chain, thereby increasing the thermal stability.

Table 2 Interaction enthalpy values of H-bond in various models

Entry	Monomer 1 (H-donor)	Monomer 2 (H-acceptor)	Interaction enthalpy (kcal mol^{-1})
1[b]	BI	BI	−13.32
2[b]	BI	BO	−9.23
3[b]	BI	BA	−10.24
4[b]	BA	BO	−9.23
5[b]	BA	BA	−6.85
6[a]	BI-BI-BI	BI-BI-BI	−4.77
7[a]	BA-BI-BI	BI-BI-BI	−10.58
8[a]	BI-BI-BI	BA-BI-BI	−10.01
9[a]	BI-BI-BA	BI-BI-BI	−12.46
10[a]	BI-BI-BI	BI-BI-BA	−12.68
11[b]	BA-BI-BA	BA-BI-BA	−14.13
12[b]	BO-BI-BO	BO-BI-BO	−13.57
13[b]	BO-BI-BA	BO-BI-BA	−13.80

[a] H-bonding enthalpy calculated *via* DFT theory. [b] H-bonding enthalpy calculated *via* DFT theory in previous work.

3.3. Mechanical properties

The mechanical properties of the terpolymer films synthesized by stepwise polymerization were investigated using the stress–strain analysis (Fig. 5a). The tensile strength at break (σ), strain at break (ε), and Young's modulus (E) were evaluated therefrom. The stress–strain curves showed a consistent increase of stress with strain up until the breakage point, corresponding to the maximum permissible strain (strain at break or ε, Table 1). The values of the mechanical properties showed regular variations with the molar compositions of PA (Fig. 5b). With the increase in mol% of PA, the value of strain at break increased from 2.3 to 12.0%, while the tensile strength decreased from 80 to 48 MPa, and the Young's modulus decreased from 3.48 to 0.40 GPa. The terpolymers with higher mol% of PA exhibited higher ε and lower E values, presumably due to their greater abundance of non-heterocyclic PA components that are expected to be more flexible than the heterocyclic PBO components.

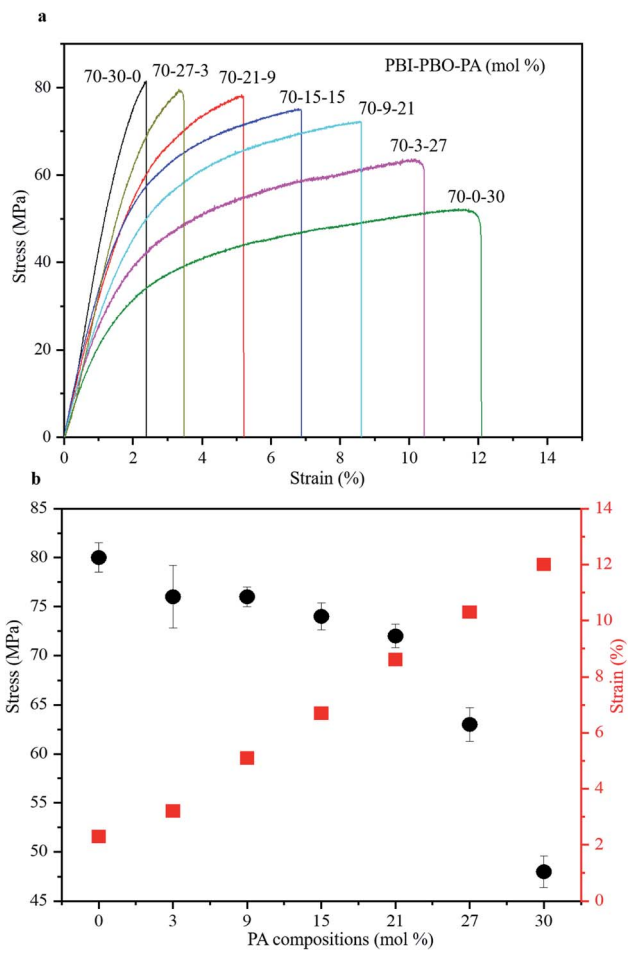

Fig. 5 Mechanical properties of terpolymers. (a) Stress–strain curves of terpolymers. (b) Tensile stress and strain values in different PA compositions.

3.4. Dielectric properties

Dielectric measurements were performed using the films obtained from P(BI-*b*-BO-A) synthesized by stepwise polymerization. The thicknesses of the terpolymer films were maintained between 7.0 to 10.0 μm for the dielectric measurements. The values of the different parameters obtained from these measurements, for the terpolymer films of different compositions, have been listed in Table 3. Fig. S2a† shows the volume

Table 3 Dielectric property indices of the terpolymers having various compositions

Polymers (PBI–PBO–PA %)	d^a (μm)	k_r^b	ρ_v^c (Ω cm)
70–30–0	7.0	2.6	6.22×10^{11}
70–27–3	8.0	2.4	6.63×10^{11}
70–21–9	10.0	3.0	1.24×10^{14}
70–15–15	6.0	2.6	2.67×10^{9}
70–9–21	7.0	2.8	3.67×10^{10}
70–3–27	8.0	2.9	5.12×10^{10}
70–0–30	9.0	3.2	4.09×10^{10}

[a] Thickness. [b] Dielectric constant. [c] Volume resistivity.

resistivity for dried P(BI-*b*-BO-A) films as a function of PA composition. The volume resistivity for terpolymer with a PA mole composition (r_{PA}) of 3% was equal to that for P(BI-*b*-BO) ($r_{PA} = 0$) at approximately 6.22×10^{11} Ω cm and it significantly increased to 1.24×10^{14} Ω cm at $r_{PA} = 9\%$, suggesting that the terpolymer changed to highly insulative. However, it suddenly decreased to 2.67×10^{10} Ω cm at $r_{PA} = 15\%$, showing that the terpolymer transforms to a low insulator where the resistivity is more than an order of magnitude lower than that of P(BI-*b*-BO) ($r_{PA} = 0$). At a region above 15%, the volume resistivity was independent of the PA composition. This drastic change in volume resistivity in the vicinity of $r_{PA} = 10\%$ is considered to be a structural transition with nano- or submicron- scale although there was no remarkable change in the appearance or transparency of the films. The structural transition was confirmed through X-ray diffraction in Fig. S3 and S4.† In electrically heterogeneous materials, even if morphologically uniform, the bulk electrical resistivity is strongly dominated by the local resistivity. Therefore, it can be considered that the low resistivity at $r_{PA} > 15\%$ was caused by the occurrence of a continuous phase with low resistivity having a wide distribution of resistance in a highly insulative matrix.[22,23] On the contrary, it can be considered that the significant increase in the resistivity at $r_{PA} < 9\%$ is due to an electrically homogeneous and high resistivity phase rapidly develops in the whole bulk of terpolymer by incorporating PA and reducing PBO. Thus, in order to understand the complex behavior of the volume resistivity, it is necessary to consider the electrical homogeneity of the resulting terpolymers.

Fig. S2b† shows the relative dielectric constant at 1 MHz for dried P(BI-*b*-BO-A) films as a function of PA ratio. The dielectric constant seems to have increased monotonously with the PA ratio although there was some variation. PBO units have a rigid aromatic backbone, resulting in a low mobility of charge in response to electric field, and the lower polarizability of the oxazoles contributed to the lower dielectric constant values for the terpolymers with higher mol% of PBO (and lower mol% of PA). It is shown below that the dielectric constant has to be considered for electrical uniformity in the same way as the resistivity. The observed dielectric constant k_{obs} for a dielectric substance consisting of several components with different dielectric property can be explained as the following equation when a parallel connection of capacitances is hypothesized,

$$\frac{1}{k_{obs}} = \sum_n \frac{\varphi_n}{k_n}, \quad (1)$$

where k_n and φ_n represent the relative dielectric constant and the fraction of each component. For the terpolymer system studied here, the observed dielectric constant k_{obs} can be explained as,

$$\frac{1}{k_{obs}} = \frac{\varphi_{PBI}}{k_{PBI}} + \frac{(1-\varphi_{PBI})(1-r_{PA})}{k_{PBO}} + \frac{(1-\varphi_{PBI})r_{PA}}{k_{PA}}, \quad (2)$$

where k_{PBI}, k_{PBO}, k_{PA} are the relative dielectric constant for neat PBI, PBO, and PA. φ_{PBI} is the volume fraction of PBI, and r_{PA} stands for the PA ratio. The experimental data was fitted by eqn (2) using a synthesis condition of $\varphi_{PBI} = 0.7$ and a measured value of $k_{PBI} = 3.4$. The result of fitting is represented as the broken red line in Fig. 5b and showed that the dielectric constant for PBO and PA was calculated to be 2.0 and 1.3, respectively. The dielectric constant for a neat PBO film after drying was measured to be 1.9, which was close to the value obtained by the fitting. However, the value of dielectric constant for PA is extremely low. Therefore, it is clearly that the observed dielectric constant cannot be explained by the parallel model of capacitors in eqn (2). The degree of crystallinity was clearly dropped off at $9\% < \varphi_{PA} < 15\%$ (Fig. S4†), therefore, it was considered that the dielectric property is strongly affected by a structural transition in local similarly to the volume resistivity.

Fig. 6 shows a plot of the dielectric constant *versus* 1% thermal degradation temperature (T_{d1}) of the obtained terpolymers alongside other commercially available polymer materials. Generally, polymer materials with low dielectric constants show relatively low thermal resistance, while those with higher dielectric constants exhibit higher thermal resistance. For example, in the same condition as terpolymer was measured, polypropylene (PP), polystyrene (PS), and poly(butyl methacrylate) (PBMA) which have low dielectric constant values (2.2, 2.6, and 2.7 respectively), also have low T_{d1} values (310, 375, and 350 °C respectively).[24–27] In contrast, polymers like poly(-phenylene sulfide) (PPS), polyimide (Kapton™), and poly(ether ether ketone) (PEEK), which exhibit high thermal resistance with high T_{d1} values (495, 500, and 525 °C respectively), also have relatively high dielectric constant values (3.8, 3.3, and 3.4, respectively). Compared to the aforementioned polymers, Zylon exhibits a relatively low dielectric constant and a high thermal resistance, presumably due to the effects of its benzoxazole structure.[28–38] The lowest dielectric constant among the terpolymers synthesized in the present work was found to be

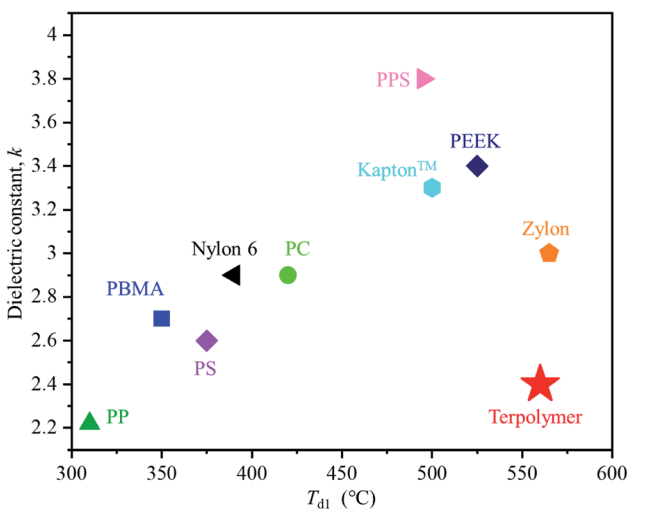

Fig. 6 Plot of dielectric constant *versus* 1% thermal degradation temperature (T_{d1}) for the terpolymer and other common commercial polymer materials:polypropylene (PP),[24,25] poly(butyl methacrylate) (PBMA),[26,27] polystyrene (PS),[28,29] Nylon 6,[30,31] polycarbonate (PC),[32] Kapton™,[33,34] polyphenylene sulfide (PPS)[35], polyether ether ketone (PEEK)[36,37] and Zylon.[38]

2.4, which is extremely low compared to that of different commercially available polymer materials. Considering its outstanding thermal resistance, we can conclude that this terpolymer exhibits the best performance among all the polymers that have been compared. Overall, the P(BI-*b*-BO-A) films can be considered reliable as thermoresistant insulators that can withstand ultrahigh operating voltages.

3.5. Coating

A coating experiment was conducted to investigate the applicability of the obtained P(BI-*b*-BO-A) as an insulator. For this, a solution of P(BI-*b*-BO-A) (mol% composition of 70–15–15) in TFA (70 mg/3 mL) was prepared, and a spiral coil of copper wire was soaked in it for 2 min. On removing from the solution and drying in air, a thin layer of the polymer was coated onto the surface of the copper wire (Fig. 7a). To investigate its dielectric performance, the coil of copper wire coated with P(BI-*b*-BO-A) was equipped with a magnet to assemble a mini motor model (Fig. 7b). The coil rotated successfully after being powered on, indicating that the coating layer functioned as an insulator. In addition, the thermal resistance of the P(BI-*b*-BO-A)-coated copper wire was compared with commercial copper wire (polyurethane enameled copper wire) by simultaneously applying a direct current (16 A, 10 V). Since the electric circuit is parallel and the length of the copper wires is same, the electric current and the resultant Joule heat should be the same for both

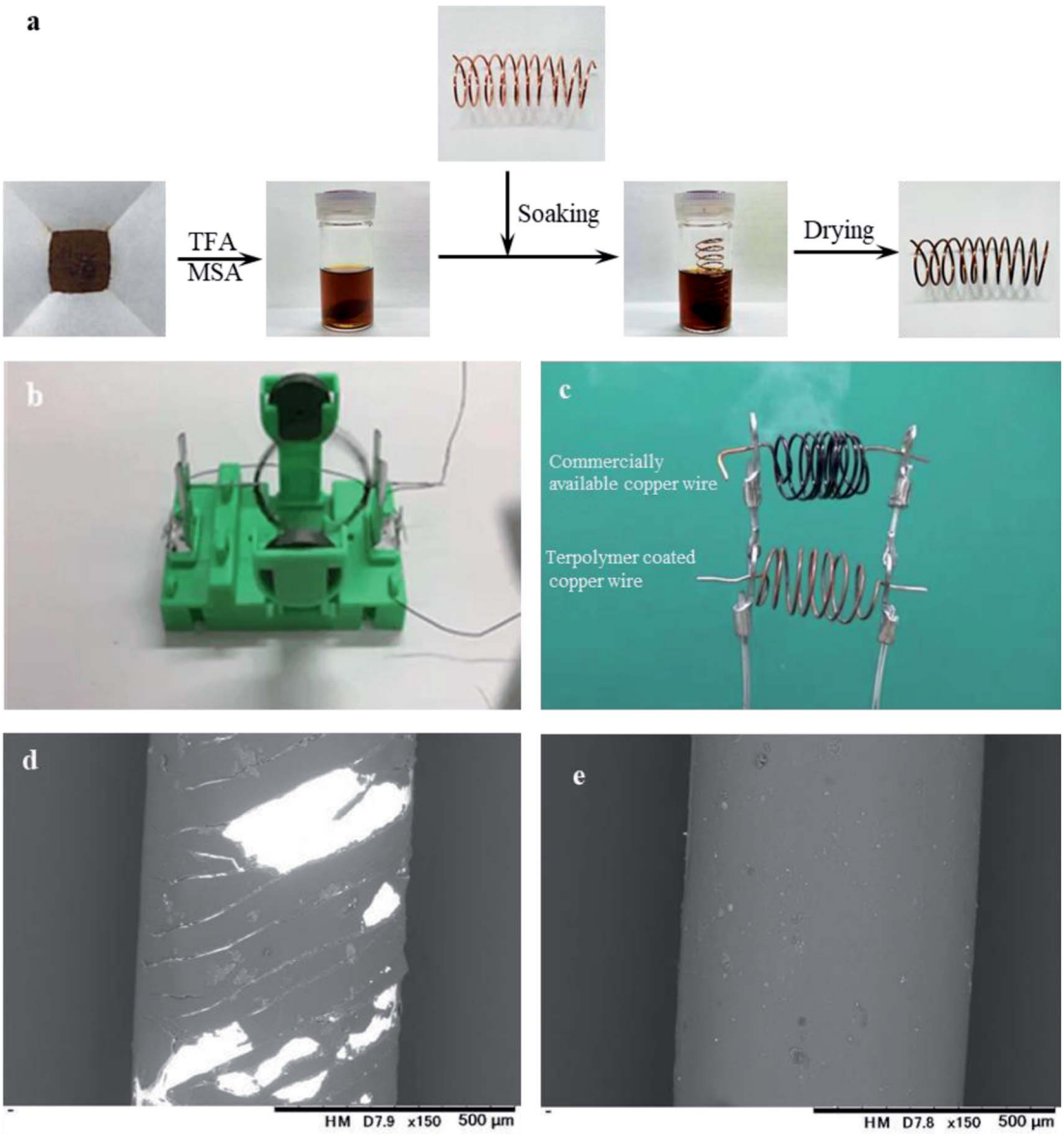

Fig. 7 a) Process of coating copper wire with terpolymer P(BI-*b*-BO-A). (b) Running experiment of motor, where the coil was assembled by a P(BI-*b*-BO-A) coated copper wire. (c) Voltage applied across the copper wires in direct current mode (upper: commercially available copper wire, lower: terpolymer coated copper wire). (d) SEM image of commercially available copper wire after applying voltage. (e) SEM image of terpolymer coated copper wire after applying voltage.

samples. When the current was gradually increased, the commercial copper wire started giving off smoke while the P(BI-*b*-BO-A)-coated one remained stable (Fig. 7c). Both coils were observed using SEM to check the condition of their surfaces after the experiment. The coating layer of the commercial copper wire presented a significant amount of damage (Fig. 7d), whereas no significant damage was observed in the P(BI-*b*-BO-A) coating layer (Fig. 7e). Thus, we can confirm that P(BI-*b*-BO-A) works as a thermostable insulating coating material.

4. Conclusions

A series of bio-based terpolymers P(BI-*b*-BO-A) having different molar compositions of PBI, PBO and PA were successfully synthesized through a stepwise polymerization procedure, which involved the pre-polymerization of DABA followed by an additional terpolymerization with AHBA and PABA. The terpolymers thus prepared exhibited outstanding thermal, mechanical, and dielectric properties. For 30 mol% of PA, the T_{d10} reached ~760 °C, which is the highest reported for any petroleum- or bio-based plastic developed so far, and is comparable to the melting temperature of light metals. DFT calculations of the hydrogen bonding enthalpy between imidazole rings revealed how the inter-chain interactions within the polymer were strengthened by incorporating PA, which could be the reason for such ultrahigh thermoresistance of the prepared terpolymers. The highest tensile strength and strain at break for the terpolymers were found to reach up to 80 MPa and 12%, respectively, which were regulated by the molar composition of the individual monomers. The strain at break increased regularly with increase in mol% of PA. The lowest dielectric constant was found to be 2.4, which is much lower than that of most commercially available thermoresistant insulators, and comparable to that of inorganic materials such as silica. Among all the compositions, the terpolymer in composition of 70–15–15 (mol%) exhibited a T_{d10} of 710 °C and a dielectric constant of 2.6, the appropriate amount of oxazole groups of PBO decreased the polarizability and the H-bond brought by PA increased the thermal stability, thus synergistically balanced the thermal stability and low-*k* performance and was considered to the most extraordinary one in all the compositions. Therefore, P(BI-*b*-BO-A) can be useful as an excellent insulating material for coating purposes, as was also confirmed from our coating experiment. Overall, we can conclude from all our results that the bio-based P(BI-*b*-BO-A) terpolymers have great potential to be utilized as coating materials for high power coil of high-speed electric vehicles, in the future.

Conflicts of interest

There are no conflicts to declare.

Acknowledgements

This work was financially supported by JAIST Research Grants (Houga) 2020. This work was also supported by the Cabinet Office, Government of Japan, Cross-ministerial Strategic Innovation Promotion Program (SIP), "Technologies for Smart Bio-industry and Agriculture" (funding agency: Bio-oriented Technology Research Advancement Institution, NARO, Grant No. 18087978), and partially supported by a JSPS KAKENHI Grant-in-aid for Scientific Research A (22H00332). The computations in this work were performed using the facilities provided by the Research Center for Advanced Computing Infrastructure at JAIST.

References

1 K. K. Sadasivuni, P. Saha, J. Adhikari, K. Deshmukh, M. B. Ahamed and J. Cabibihan, *Polym. Compos.*, 2020, **41**, 32–59.
2 X.-Y. Zhao and H.-J. Liu, *Polym. Int.*, 2010, **59**, 597–606.
3 M. G. A. Vieira, M. A. Da Silva, L. O. Dos Santos and M. M. Beppu, *Eur. Polym. J.*, 2011, **47**, 254–263.
4 J. Rajesh Banu, S. Kavitha, R. Yukesh Kannah, T. Poornima Devi, M. Gunasekaran, S.-H. Kim and G. Kumar, *Bioresour. Technol.*, 2019, **290**, 121790.
5 S. Park, H. Jeon, H. Kim, S. Shin, S. Choy, D. S. Hwang, J. M. Koo, J. Jegal, S. Y. Hwang, J. Park and D. X. Oh, *Nat. Commun.*, 2019, **10**, 2601.
6 O. Valerio, M. Misra and A. K. Mohanty, *RSC Adv.*, 2017, **7**, 38594–38603.
7 T. P. Dawin, Z. Ahmadi and F. A. Taromi, *Prog. Org. Coat.*, 2018, **119**, 23–30.
8 Q. Li, F.-Z. Yao, Y. Liu, G. Zhang, H. Wang and Q. Wang, *Annu. Rev. Mater. Res.*, 2018, **48**, 219–243.
9 A. Nag, M. A. Ali, M. Watanabe, M. Singh, K. Amornwachirabodee, S. Kato, T. Mitsumata, K. Takada and T. Kaneko, *Polym. Degrad. Stab.*, 2019, **162**, 29–35.
10 K. L. Gordon, J. H. Kang, C. Park, P. T. Lillehei and J. S. Harrison, *J. Appl. Polym. Sci.*, 2012, **125**, 2977–2985.
11 Z.-J. Liu, C.-G. Yin, V. Cecen, J.-C. Fan, P.-H. Shi, Q.-J. Xu and Y.-L. Min, *Polymer*, 2019, **179**, 121613.
12 D. Li, D. Shi, Y. Xia, L. Qiao, X. Li and H. Zhang, *ACS Appl. Mater. Interfaces*, 2017, **9**, 8742–8750.
13 A. Nag, M. A. Ali, H. Kawaguchi, S. Saito, Y. Kawasaki, S. Miyazaki, H. Kawamoto, D. T. N. Adi, K. Yoshihara, S. Masuo, Y. Katsuyama, A. Kondo, C. Ogino, N. Takaya, T. Kaneko and Y. Ohnishi, *Adv. Sustainable Syst.*, 2020, 2000193.
14 J. D. Moon, A. T. Bridge, C. D'Ambra, B. D. Freeman and D. R. Paul, *J. Membr. Sci.*, 2019, **582**, 182–193.
15 S. W. Chuang, S. L. C. Hsu and Y. H. Liu, *J. Membr. Sci.*, 2007, **305**, 353–363.
16 F. Yao, W. Xie, M. Yang, H. Zhang, H. Gu, A. Du, N. Naik, D. P. Young, J. Lin and Z. Guo, *Mater. Today Phys.*, 2021, **21**, 100502.
17 A. Nag, M. A. Ali, A. Singh, R. Vedarajan, N. Matsumi and T. Kaneko, *J. Mater. Chem. A*, 2019, **7**, 4459–4468.
18 A. A. Arbuzov, V. E. Muradyan, B. P. Tarasov, E. A. Sokolov and S. D. Babenko, *Russ. J. Phys. Chem. A*, 2016, **90**, 907–910.
19 T. Yanai, D. P. Tew and N. C. Handy, *Chem. Phys. Lett.*, 2004, **393**, 51–57.

20 D. E. Woon and T. H. Dunning, *J. Chem. Phys.*, 1993, **98**, 1358–1371.
21 S. Simon, M. Duran and J. J. Dannenberg, *J. Chem. Phys.*, 1996, **105**, 11024–11031.
22 X. Xu, Q. Fu, H. Gu, Y. Guo, H. Zhou, J. Zhang, D. Pan, S. Wu, M. Dong and Z. Guo, *Polymer*, 2020, **188**, 122129.
23 P. Wang, L. Yang, S. Gao, X. Chen, T. Cao, C. Wang, H. Liu, X. Hu, X. Wu and S. Feng, *Adv. Compos. Hybrid Mater.*, 2021, **4**, 639–646.
24 X. Yuan, Y. Matsuyama and T. C. M. Chung, *Macromolecules*, 2010, **43**, 4011–4015.
25 E. Esmizadeh, C. Tzoganakis and T. H. Mekonnen, *Polymers*, 2020, **12**, 1627.
26 S. Strella and R. Zand, *J. Polym. Sci.*, 1957, **25**, 105–114.
27 Z. Czech, K. Agnieszka, P. Ragańska and A. Antosik, *J. Therm. Anal. Calorim.*, 2015, **119**, 1157–1161.
28 S. Yu, P. Hing and X. Hu, *J. Appl. Phys.*, 2000, **88**, 398–404.
29 T. ARII, *J. Mass Spectrom. Soc. Jpn.*, 2003, **51**, 235–241.
30 H. Gu, X. Xu, J. Cai, S. Wei, H. Wei, H. Liu, D. P. Young, Q. Shao, S. Wu, T. Ding and Z. Guo, *Chem. Commun.*, 2019, **55**, 10068–10071.
31 Matweb, Overview of Materials for Nylon 6/66, **https://www.matweb.com/search/datasheet_print.aspx?matguid=26386631ec1b49eeba62c80a49730dc4**, accessed: March 2021.
32 Overview of materials for Polycarbonate, High Heat, **https://www.matweb.com/search/DataSheet.aspx?MatGUID=bfcedbb55b164a68a93acfa854fa2fe0**, accessed: March 2021.
33 A. C. Lua and J. Su, *Polym. Degrad. Stab.*, 2006, **91**, 144–153.
34 T. Kuroki, Y. Tanaka, T. Hokudoh and K. Yabuki, *J. Appl. Polym. Sci.*, 1997, **65**, 1031–1036.
35 W. Tanthapanichakoon, M. Furuuchi, K. Nitta, M. Hata, S. Endoh and Y. Otani, *Polym. Degrad. Stab.*, 2006, **91**, 1637–1644.
36 H. Sun, Y. Lv, C. Zhang, X. Zuo, M. Li, X. Yue and Z. Jiang, *RSC Adv.*, 2018, **8**, 7753–7760.
37 P. Patel, T. R. Hull, R. W. McCabe, D. Flath, J. Grasmeder and M. Percy, *Polym. Degrad. Stab.*, 2010, **95**, 709–718.
38 ToyoboZylon® **https://www.matweb.com/search/DataSheet.aspx?MatGUID=140045b4f06c4aea89f8900f4c7bb4fc**, accessed: March 2021.